Computers and Concrete, *Vol. 19, No. 6 (2017) 677-687*
DOI: https://doi.org/10.12989/cac.2017.19.6.677

Nonlinear stability of non-axisymmetric functionally graded reinforced nano composite microplates

Abbas Loghman, Ali Ghorbanpour Arani and Ali Akbar Mosallaie Barzoki*

Department of Solid Mechanics, Faculty of Mechanical Engineering, University of Kashan, Kashan, Iran

(Received October 22, 2016, Revised February 12, 2017, Accepted February 17, 2017)

Abstract. The nonlinear buckling response of nano composite anti-symmetric functionally graded polymeric microplate reinforced by single-walled carbon nanotubes (SWCNTs) rested on orthotropic elastomeric foundation with temperature dependent properties is investigated. For the carbon-nanotube reinforced composite (CNTRC) microplate, a uniform distribution (UD) and four types of functionally graded (FG) distribution are considered. Based on orthotropic Mindlin plate theory, von Kármán geometric nonlinearity and Hamilton's principle, the governing equations are derived. Generalized differential quadrature method (GDQM) is employed to calculate the non-linear buckling response of the plate. Effects of FG distribution type, elastomeric foundation, aspect ratio (thickness to width ratio), boundary condition, orientation of foundation orthotropy and temperature are considered. The results are validated. It is found that the critical buckling load without elastic medium is significantly lower than considering Winkler and Pasternak medium.

Keywords: nonlinear stability; reinforced microplates; non-axisymmetric functionally graded materials; Pasternak shear foundation

1. Introduction

Fiber-reinforced composites are extensively used in various fields of modern engineering due to their particular structural advantages. Comprehensive understanding of the mechanical behavior of composite plate is crucial to assure the integrity of these structures during their service life. A reasonable number of studies have been conducted on predicting optimum laminate configurations for enhancing the load capacity of composite structures. Stability study is important in engineering practice. Due to significance of buckling and stability, there are so many researchers around the world who are working on different structures such as beams, shells and plates under various loading combinations (Lee and Reddy 2010, Piovan *et al*. 2012).

Due to the recent developments on buckling behavior of nano-composite structures, Mosallaie *et al*. (2012) have studied the electro-thermo-mechanical torsional buckling response of a piezoelectric polymeric cylindrical shell reinforced by double walled boron nitride nanotubes (BNNTs) with an elastic core. Later, Mosallaie *et al*. (2013) and Ghorbanpour *et al*. (2014) improved their stability studies by considering nonlinear buckling response of embedded piezoelectric cylindrical shell reinforced by BNNT under electro-thermo-mechanical loadings.

Reddy (1984), using finite element analyses, investigated the effect of transverse shear deformation on deflection and stresses of laminated composite plates subjected to uniformly distributed load. Ferreira *et al*. (2003) studied composite plates using higher-order shear deformation theory and a finite point formulation based on the multiquadric radial basis function method.

An analytic solution for static behaviors of antisymmetric angle-ply composite and sandwich plates has been presented by Swaminathan and Ragounadin (2004). The nonlinear bending behavior of simply supported functionally graded (FG) nanocomposite plates reinforced by single-walled carbon nanotubes (SWCNTs) was studied by Shen (2009). Transverse uniform or sinusoidal load in thermal environments was considered. A rectangular laminated composite thick plate resting on nonlinear two-parameter elastic foundation with cubic nonlinearity was analyzed by Baltacıoğlu *et al*. (2011).

They applied first-order shear deformation theory (FSDT), for the plate formulation and illustrated the effects of foundation as well as geometric parameters of the plate on displacements considering the nonlinear parameters. Jafari *et al*. (2012) studied on the mechanical buckling of a FG nanocomposite rectangular plate reinforced by aligned and straight SWCNTs subjected to uniaxial and biaxial in-plane loadings. Because of the excellent mechanical, physical and electronic properties of CNTs (Salvetat and Rubio 2002), CNTs are considered to be the best candidates for the reinforcement of polymer composites (Esawi and Farag 2007, Fiedler *et al*. 2006). In microelectromechanical systems (MEMS) and nanoelectromechanical systems (NEMS) carbon-nanotube reinforced composite (CNTRC) are extensively used.

Stability of such structures is important. Due to randomly distribution of nano tubes as reinforcement the resulting mechanical, thermal, or physical properties of particle reinforced composites are traditionally considered to be uniform spatially at the macroscopic level. Buckling

*Corresponding author, Ph.D.
E-mail: ali.mosallaie@gmail.com

http://www.techno-press.org/?journal=cac&subpage=8
ISSN: 1598-8198 (Print), 1598-818X (Online)

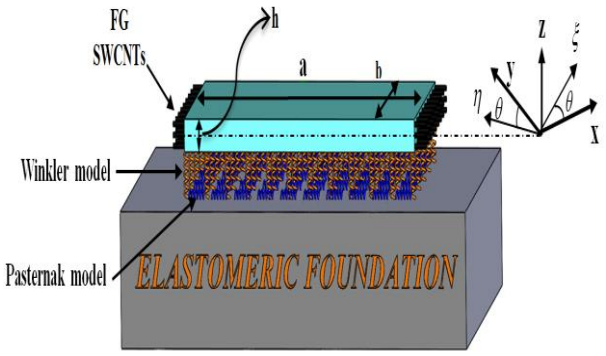

Fig. 1 Geometry of the CNTRC microplate resting on an orthotropic elastomeric temperature-dependent foundation

analysis of variable angle tow, variable thickness panels considering transverse shear effects have been developed by Groh and Weaver (2014). The idea of investigating the effects of two-dimensional fiber orientations with their associated doubly curved topologies was proposed. Dynamic buckling analysis of delaminated composite plates using semi-analytical finite strip method was carried out by Ovesy *et al.* (2015). Nonuniform distribution of the reinforcement phase in functionally (FGM) graded materials, in which the micro structural details are spatially varied, have been considered by Ghorbanpour *et al.* (2011, 2012a).

Microstructural management of nanocomposite plate can be employed to improve buckling behavior of FGM structures. The buckling behavior of thick plates has attracted considerable attention in recent years. An exact solution for the buckling response of rectangular Mindlin plates resting on elastic foundation subjected to uniformly and linearly distributed in-plane loadings has been investigated by Akhavan *et al.* (2009). Stability of homogeneous plate resting on elastic foundation was presented by Morozov and Tovstik (2010). Nonlinear vibration, bending and post buckling response of SWCNTs resting on a two-parameter elastomeric foundation in the presence of thermal environments was studied by Shen and Zhang (2011).

The buckling behavior of heated functionally graded material (FGM) annular plates on an elastic foundation was studied analytically by Kiani and Eslami (2013). A conventional Pasternak-type elastic foundation is assumed to be in contact with plate during deformation. Sinusoidal shear deformation theory was employed by Huu and Thuc (2013) for bending, buckling, and vibration analysis of FG plates. This theory accounts for the sinusoidal distribution of transverse shear stress, and satisfies the free transverse shear stress conditions on the top and bottom surfaces of the plate without using shear correction factor. Mosallaie *et al.* (2015) have investigated temperature-dependent nonlocal buckling response of microplates rested on elastomeric medium. Their results are illustrated for different boundary conditions versus nonlocal parameter.

In the present study, nonlinear stability of non-axisymmetric functionally graded SWCNT-reinforced polymer based plates considering temperature-dependent properties rested on elastomeric foundation has been studied. The heat conduction problem was solved and the obtained temperature distribution was considered in governing equation. For CNTRC plate, a uniform distribution (UD) and four types of FG distribution involving the non-axisymmetric type of FG patterns (NAFG) of SWCNT reinforcements are assumed. The mixture rule is used to obtain the equivalent material properties of FG-CNTRC plate. The nonlinear governing equations are derived using Hamilton's principal and Mindlin orthotropic plate theory. The nonlinear buckling load of the FG-CNTRC polymeric microplate is obtained by applying generalized differential quadrature method (GDQM). The results are presented for the buckling load versus plate length considering the effects of, elastomeric medium, aspect ratio, temperature gradient, boundary conditions, orientation of foundation orthotropy.

2. Mixture model of CNT-reinforced polymeric composite microplate

As shown in Fig. 1, a CNTRC microplate with length a, width b and thickness h is considered. The CNTRC plate is rested an orthotropic elastomeric temperature-dependent medium which is simulated by K_W, G_ξ and G_η corresponding to Winkler foundation parameter, shear foundation parameters in ξ and η directions, respectively. Based on the distribution of CNTs in the polymer matrix, five types of CNTRC plates are considered.

These are designated by UD for uniform, FGA, FGO, FGX for three symmetrical middle layer types of FG distributions and NAFG for a non-axisymmetric functionally graded distribution. Eqs. (1)-(5) are mathematical representation of all previous mentioned distributions. In order to obtain the equivalent material properties of two-phase nano composites (i.e., polymer as matrix and CNT as reinforcement), the rule of mixture is applied by Esawi and Farag (2007).

The uniform and four types of FG distributions of the CNTs along the thickness direction of the CNTRC plates take the following forms

$$UD: \quad V_{CNT} = V_{CNT}^{*}, \tag{1}$$

$$FGA: \ V_{CNT}(z) = \left(1 - \frac{2z}{h}\right) V_{CNT}^{*}, \tag{2}$$

$$FGO: \ V_{CNT}(z) = 2\left(1 - \frac{2|z|}{h}\right) V_{CNT}^{*}, \tag{3}$$

$$FGX: \ V_{CNT}(z) = 2\left(\frac{2|z|}{h}\right) V_{CNT}^{*}, \tag{4}$$

$$NAFG: \ V_{CNT}(z) = \left(1 - \frac{h}{z}\right) V_{CNT}^{*}, \tag{5}$$

where,

$$V_{CNT}^{*} = \frac{w_{CNT}}{w_{CNT} + (\rho_{CNT}/\rho_m) - (\rho_{CNT}/\rho_m) w_{CNT}}, \tag{6}$$

where w_{CNT}, ρ_m and ρ_{CNT} are the mass fraction of the CNT, the densities of the matrix and CNT, respectively. Similarly, the thermal expansion coefficients in the longitudinal and transverse directions respectively (α_{11} and α_{22}), Poisson's ratio (ν_{12}) and the density (ρ) of the CNTRC plates can be determined as (Mosallaie *et al.* 2015)

$$\nu_{12} = V_{CNT}^{*}\nu_{r12} + V_m\nu_m, \tag{7}$$

$$\rho = V_{CNT}^{*}\rho_r + V_m\rho_m, \tag{8}$$

$$\alpha_{11} = V_{CNT}^{*}\alpha_{r11} + V_m\alpha_m, \tag{9}$$

$$\alpha_{22} = (1+\nu_{r12})V_{CNT}\alpha_{r22} + (1+\nu_m)V_m\alpha_m - \nu_{12}\alpha_{11}, \tag{10}$$

where ν_{r12} and ν_m are Poisson's ratios of the CNT and matrix, respectively. In addition, α_{r11}, α_{r22} and α_m are the thermal expansion coefficients of the CNT and matrix, respectively. It should be noted that ν_{12} is assumed as constant over the thickness of the FG-CNTRC plates.

3. Heat conduction problem

Assume a FG-CNTRC polymeric microplate where the temperature at the up and down surfaces are T_u and T_d, respectively. The governing equation for the steady-state one-dimensional Fourier heat conduction equation, in the absence of heat source, becomes

$$\begin{cases} \dfrac{d}{dz}\left(K(z)\dfrac{dT}{dz}\right) = 0 & -h/2 < z < h/2 \\ T = T_d & z = -h/2 \\ T = T_u & z = h/2 \end{cases} \tag{11}$$

where $K=K(z)$, is the thermal conductivity. Similar to the coefficients of elastic moduli and thermal expansion, the coefficient of heat conduction is also assumed as a function of variable z coordinate based on the volume content of the constituent.

$$K(z) = V_{CNT}^{*}K_r + V_mK_m, \tag{12}$$

Eq. (11) can be solved by using a polynomial power series expansion given as: (Fiorenzo 2015)

$$T(z) = T_d + \frac{(T_u - T_d)}{J}V_{CNT}^{*}\sum_{i=0}^{H_T}\left[(-1)^i\frac{V_{CNT}^{*\,i}(K_r - K_m)}{(i+1)K_m}\right] \tag{13}$$

where H_T is the number of series' terms, which, for the case of non-uniform temperature rise, is obtained from a convergence study. Temperature is obtained as function of V^{*}_{CNT} which is dependent on z coordinate. J is defined as follows

$$J = \sum_{i=0}^{H_T}\left[(-1)^i\frac{(K_r - K_m)^i}{(i+1)K_m}\right] \tag{14}$$

4. Constitutive equations for CNTRC polymeric microplate

4.1 Orthotropic stress-strain relations

The constitutive equation for stresses σ and strains ε matrix in thermal environment may be written as follows

$$\begin{Bmatrix}\sigma_{xx}\\ \sigma_{yy}\\ \sigma_{yz}\\ \sigma_{zx}\\ \sigma_{xy}\end{Bmatrix} = \begin{bmatrix} C_{11} & C_{12} & 0 & 0 & 0 \\ C_{21} & C_{22} & 0 & 0 & 0 \\ 0 & 0 & C_{44} & 0 & 0 \\ 0 & 0 & 0 & C_{55} & 0 \\ 0 & 0 & 0 & 0 & C_{66} \end{bmatrix}\begin{Bmatrix}\varepsilon_{xx} - \alpha_{xx}T\\ \varepsilon_{yy} - \alpha_{yy}T\\ \gamma_{yz}\\ \gamma_{xz}\\ \gamma_{xy}\end{Bmatrix}, \tag{15}$$

where $C_{ij}(i,\ j=1,2,\ldots,6)$ denotes temperature-dependent elastic coefficients which are dependent on z direction and temperature. Note that C_{ij} and α_{xx}, α_{yy} may be obtained using rule of mixture (i.e., Eqs. (1)-(10)).

4.2 Nonlinear mindlin plate theory

Displacement field according Mindlin plate theory, can be represented as (Reddy (1984))

$$\begin{Bmatrix}u_x\\ u_y\\ u_z\end{Bmatrix}(x,y,z,t) = \begin{bmatrix}1&0&0\\0&1&0\\0&0&1\end{bmatrix}\begin{Bmatrix}u\\ v\\ w\end{Bmatrix}(x,y,t) + \begin{bmatrix}z&0&0\\0&z&0\\0&0&0\end{bmatrix}\begin{Bmatrix}\psi_x(x,y)\\ \psi_y(x,y)\\ 0\end{Bmatrix}, \tag{16}$$

where $(u_x,\ u_y,\ u_z)$ denote the displacement components at an arbitrary point (x,y,z) in the plate, and (u,v,w) are the displacement of a material point at (x,y) on the mid-plane (i.e., z=0) of the plate along the x-, y-, and z-directions, respectively; the rotations of the normal to the mid-plane about x- and y-directions are expressed by $\psi_x(x,y)$ and $\psi_y(x,y)$, respectively.

Considering nonlinear von Kármán strains associated with displacement field, which was mentioned on Eq. (16), can be expressed as

$$\varepsilon_{xx} = \frac{\partial}{\partial x}\left(u(x,y)\right) + z\frac{\partial}{\partial x}\left(\psi_x(x,y)\right) + \frac{1}{2}\left(\frac{\partial}{\partial x}w(x,y)\right)^2 \tag{17}$$

$$\varepsilon_{yy} = \frac{\partial}{\partial y}\left(v(x,y)\right) + z\frac{\partial}{\partial y}\left(\psi_y(x,y)\right) + \frac{1}{2}\left(\frac{\partial}{\partial y}w(x,y)\right)^2 \tag{18}$$

$$\gamma_{yz} = \frac{\partial}{\partial y}w(x,y) + \psi_y(x,y) \tag{19}$$

$$\gamma_{xz} = \frac{\partial}{\partial x}w(x,y) + \psi_x(x,y) \tag{20}$$

$$\gamma_{xy} = \frac{\partial}{\partial y}u(x,y) + \frac{\partial}{\partial x}v(x,y) + \frac{\partial}{\partial x}w(x,y).\frac{\partial}{\partial y}w(x,y) + z.\left(\frac{\partial}{\partial y}\psi_x(x,y) + \frac{\partial}{\partial x}\psi_y(x,y)\right), \tag{21}$$

where $(\varepsilon_{xx},\ \varepsilon_{yy})$ are representing the normal strain components and $(\gamma_{yz},\ \gamma_{xz},\ \gamma_{xy})$ are the shear strain components.

4.3 Energy equations

The energy method is employed to obtain the

equilibrium equations. The total potential energy, V, of the CNTRC plate is the sum of strain energy, U, and the work done by the elasomeric medium, W.

4.3.1 Strain energy

The total strain energy can be obtained integrating the strain energy density over the entire volume of the microplate as

$$U=\frac{1}{2}\int_A\int_{-h/2}^{h/2}\left(\sigma_{xx}\varepsilon_{xx}+\sigma_{yy}\varepsilon_{yy}+\sigma_{xy}\gamma_{xy}+\sigma_{xz}\gamma_{xz}+\sigma_{yz}\gamma_{yz}\right)dz\,dA \quad (22)$$

where, A is surface element.

Substituting stresses from Eq. (15) and strains from Eqs. (17)-(21) into Eq. (22) and integrating with respect to z yields

$$\begin{aligned}U=\frac{1}{2}\int_A\Bigg(&N_{xx}\left(\frac{\partial u(x,y)}{\partial x}+\frac{1}{2}\left(\frac{\partial w(x,y)}{\partial x}\right)^2\right)+N_{yy}\left(\frac{\partial v(x,y)}{\partial y}+\frac{1}{2}\left(\frac{\partial w(x,y)}{\partial y}\right)^2\right)\\&+N_{yz}\left(\frac{\partial w(x,y)}{\partial y}+\psi_y(x,y)\right)+N_{xz}\left(\frac{\partial w(x,y)}{\partial x}+\psi_x(x,y)\right)\\&+N_{xy}\left(\frac{\partial u(x,y)}{\partial y}+\frac{\partial v(x,y)}{\partial x}+\frac{\partial w(x,y)}{\partial x}\frac{\partial w(x,y)}{\partial y}\right)+M_{xx}\frac{\partial\psi_x(x,y)}{\partial x}\\&+M_{yy}\frac{\partial\psi_y(x,y)}{\partial x}+M_{xy}\left(\frac{\partial\psi_x(x,y)}{\partial y}+\frac{\partial\psi_y(x,y)}{\partial x}\right)\Bigg)dxdy\end{aligned} \quad (23)$$

where the stress resultant-displacement relations can be written as

$$\begin{bmatrix}N_{xx}&M_{xx}\\N_{yy}&M_{yy}\\N_{xy}&M_{xy}\end{bmatrix}=\int_{-h/2}^{h/2}\begin{bmatrix}\sigma_{xx}\\\sigma_{yy}\\\sigma_{xy}\end{bmatrix}(1,z)dz, \quad (24)$$

$$\begin{bmatrix}Q_x\\Q_y\end{bmatrix}=K\int_{-h/2}^{h/2}\begin{bmatrix}\sigma_{xz}\\\sigma_{yz}\end{bmatrix}dz, \quad (25)$$

in which, K is the shear correction coefficient.

4.3.2 External work

The external work due to orthotropic temperature-dependent elastomeric medium and a uniform load on upper surface of the CNTRC microplate can be written as

$$W=\int_0^a P\ w(x,y)dx, \quad (26)$$

Where P is related to orthotropic elastomeric medium. Orthotropic elastomeric foundation can be expressed as (Shen 2009, Kutlu and Omurtag 2012)

$$\begin{aligned}P=K_W w&-G_\xi\left(\cos^2\theta\frac{\partial^2 w}{\partial x^2}+2\cos\theta\sin\theta\frac{\partial^2 w}{\partial x\,\partial y}+\sin^2\theta\frac{\partial^2 w}{\partial y^2}\right)\\&-G_\eta\left(\sin^2\theta\frac{\partial^2 w}{\partial x^2}-2\sin\theta\cos\theta\frac{\partial^2 w}{\partial x\,\partial y}+\cos^2\theta\frac{\partial^2 w}{\partial y^2}\right),\end{aligned} \quad (27)$$

where angle θ describes the local ξ direction of orthotropic foundation with respect to the global x-axis of the plate as shown in Fig. 1. Since the elastomeric medium is relatively soft, the foundation stiffness K_w may be expressed by (Shen 2009, Kutlu and Omurtag 2012)

$$K_W=\frac{E_0}{4L(1-\nu_0^2)(2-c_1)^2}\left[5-\left(2\gamma_1^2+6\gamma_1+5\right)\exp(-2\gamma_1)\right], \quad (28)$$

where

$$c_1=(\gamma_1+2)\exp(-\gamma_1), \quad (29)$$

$$\gamma_1=\frac{H_s}{L}, \quad (30)$$

$$E_0=\frac{E_s}{(1-\nu_s^2)}, \quad (31)$$

$$\nu_0=\frac{\nu_s}{(1-\nu_s)}, \quad (32)$$

where E_s, ν_s, H_s are Young's modulus, Poisson's ratio and depth of the foundation, respectively. In this paper, E_s is assumed to be temperature-dependent while ν_s is assumed to be a constant (Swaminathan and Ragounadin 2004).

5. Governing equations

The governing equations can be derived by Hamilton's principal as follows

$$\delta\int_0^t(W-U)dt=0\Rightarrow\int_0^t(\delta W-\delta U)dt=0. \quad (33)$$

Substituting Eqs. (23) and (26) into Eq. (33) yields the following governing equations

$$\delta u:\frac{\partial N_{xx}}{\partial x}+\frac{\partial N_{xy}}{\partial y}=0, \quad (34)$$

$$\delta v:\frac{\partial N_{xy}}{\partial x}+\frac{\partial N_{yy}}{\partial y}=0, \quad (35)$$

$$\delta w:\frac{\partial N_{xz}}{\partial x}+\frac{\partial N_{yz}}{\partial y}+\frac{\partial}{\partial x}\left(N_{xx}\frac{\partial w}{\partial x}+N_{xy}\frac{\partial w}{\partial y}\right)+\frac{\partial}{\partial y}\left(N_{xy}\frac{\partial w}{\partial x}+N_{yy}\frac{\partial w}{\partial y}\right)+P=0. \quad (36)$$

$$\delta\psi_x:\frac{\partial M_{xx}}{\partial x}+\frac{\partial M_{xy}}{\partial y}-Q_x=0, \quad (37)$$

$$\delta\psi_y:\frac{\partial M_{xy}}{\partial x}+\frac{\partial M_{yy}}{\partial y}-Q_y=0, \quad (38)$$

Substituting Eq. (15) and Eqs. (17)-(21) into Eqs. (24) and (25), the stress resultant-displacement relations can be obtained as follows

$$N_{xx}=S_{11}.\frac{\partial}{\partial x}u(x,y)+R_{11}.\frac{\partial}{\partial x}\psi_x(x,y)+\frac{1}{2}.S_{11}.\left(\frac{\partial}{\partial x}w(x,y)\right)^2 +S_{12}.\frac{\partial}{\partial y}v(x,y)+R_{12}.\frac{\partial}{\partial y}\psi_y(x,y)+\frac{1}{2}.S_{12}.\left(\frac{\partial}{\partial y}w(x,y)\right)^2-N_{xx}^T \tag{39}$$

$$N_{yy}=S_{12}.\frac{\partial}{\partial x}u(x,y)+R_{12}.\frac{\partial}{\partial x}\psi_x(x,y)+\frac{1}{2}.S_{12}.\left(\frac{\partial}{\partial x}w(x,y)\right)^2 +S_{22}.\frac{\partial}{\partial y}v(x,y)+R_{22}.\frac{\partial}{\partial y}\psi_y(x,y)+\frac{1}{2}.S_{22}.\left(\frac{\partial}{\partial y}w(x,y)\right)^2-N_{yy}^T \tag{40}$$

$$N_{xy}=S_{66}.\left(\frac{\partial}{\partial y}u(x,y)+\frac{\partial}{\partial x}v(x,y)\right)+R_{66}.\left(\frac{\partial}{\partial y}\psi_x(x,y)+\frac{\partial}{\partial x}\psi_y(x,y)\right) +S_{66}.\left(\frac{\partial}{\partial y}w(x,y).\frac{\partial}{\partial x}v(x,y)\right) \tag{41}$$

$$Q_x=S_{55}.\left(\psi_x(x,y)+\frac{\partial}{\partial x}w(x,y)\right) \tag{42}$$

$$Q_y=S_{44}.\left(\psi_y(x,y)+\frac{\partial}{\partial y}w(x,y)\right) \tag{43}$$

$$M_{xx}=H_{11}.\frac{\partial}{\partial x}\psi_x(x,y)+R_{11}.\left(\frac{\partial}{\partial x}u(x,y)+\frac{1}{2}.\left(\frac{\partial}{\partial x}w(x,y)\right)^2\right) +H_{12}.\frac{\partial}{\partial y}\psi_y(x,y)+R_{12}.\left(\frac{\partial}{\partial y}v(x,y)+\frac{1}{2}.\left(\frac{\partial}{\partial y}w(x,y)\right)^2\right) \tag{44}$$

$$M_{yy}=H_{12}.\frac{\partial}{\partial x}\psi_x(x,y)+R_{12}.\left(\frac{\partial}{\partial x}u(x,y)+\frac{1}{2}.\left(\frac{\partial}{\partial x}w(x,y)\right)^2\right) +H_{12}.\frac{\partial}{\partial y}\psi_y(x,y)+R_{22}.\left(\frac{\partial}{\partial y}v(x,y)+\frac{1}{2}.\left(\frac{\partial}{\partial y}w(x,y)\right)^2\right) \tag{45}$$

$$M_{xy}=H_{66}.\left(\frac{\partial}{\partial y}\psi_x(x,y)+\frac{\partial}{\partial x}\psi_y(x,y)\right) +R_{66}.\left(\frac{\partial}{\partial y}u(x,y)+\frac{\partial}{\partial x}v(x,y)+\left(\frac{\partial}{\partial x}w(x,y)\right).\left(\frac{\partial}{\partial y}w(x,y)\right)\right), \tag{46}$$

where,

$$S_{ij}=\int_{-h/2}^{h/2}C_{ij}dz, \qquad (i,j=1,2,6) \tag{47}$$

$$R_{ij}=\int_{-\frac{h}{2}}^{\frac{h}{2}}Q_{ij}.z\,dz, \qquad (i,j=1,2,6) \tag{48}$$

$$H_{ij}=\int_{-\frac{h}{2}}^{\frac{h}{2}}Q_{ij}.z^2dz, \qquad (i,j=1,2,6) \tag{49}$$

Furthermore, $\left(N_{xx}^T,N_{yy}^T\right)$ and $\left(M_{xx}^T,M_{yy}^T\right)$ are thermal force and thermal moment resultants, respectively, and are given by

$$\begin{Bmatrix}N_{xx}^T\\N_{yy}^T\end{Bmatrix}=\int_{-h/2}^{h/2}\begin{Bmatrix}C_{11}.\alpha_{11}+C_{12}.\alpha_{22}\\C_{21}.\alpha_{11}+C_{22}.\alpha_{22}\end{Bmatrix}.T\,dz, \tag{50}$$

$$\begin{Bmatrix}M_{xx}^T\\M_{yy}^T\end{Bmatrix}=\int_{-h/2}^{h/2}\begin{Bmatrix}C_{11}.\alpha_{11}+C_{12}.\alpha_{22}\\C_{21}.\alpha_{11}+C_{22}.\alpha_{22}\end{Bmatrix}.T\cdot z dz, \tag{51}$$

Substituting Eqs. (39)-(51) into Eqs. (34)-(38), the governing equations can be written as follows

$$\begin{aligned}\delta u:\;&S_{11}\left(\frac{\partial^2}{\partial x^2}u(x,y)+\frac{\partial}{\partial x}w(x,y)\frac{\partial^2}{\partial x^2}w(x,y)\right)+S_{12}\left(\frac{\partial^2}{\partial x\,\partial y}v(x,y)\right.\\&\left.+\frac{\partial}{\partial y}w(x,y)\frac{\partial^2}{\partial x\,\partial y}w(x,y)\right)+S_{66}\left(\frac{\partial^2}{\partial y^2}u(x,y)+\frac{\partial^2}{\partial x\,\partial y}v(x,y)\right.\\&\left.+\frac{\partial}{\partial y}w(x,y)\frac{\partial^2}{\partial x\,\partial y}w(x,y)+\frac{\partial}{\partial x}w(x,y)\frac{\partial^2}{\partial y^2}w(x,y)\right)\\&+R_{11}\frac{\partial^2}{\partial x^2}\psi_x(x,y)+R_{12}\frac{\partial^2}{\partial x\,\partial y}\psi_y(x,y)=0,\end{aligned} \tag{52}$$

$$\begin{aligned}\delta v:\;&S_{12}\left(\frac{\partial^2}{\partial x\,\partial y}u(x,y)+\frac{\partial}{\partial x}w(x,y)\frac{\partial^2}{\partial x\,\partial y}w(x,y)\right)+S_{22}\left(\frac{\partial^2}{\partial y^2}v(x,y)\right.\\&\left.+\frac{\partial}{\partial y}w(x,y)\frac{\partial^2}{\partial y^2}w(x,y)\right)+S_{66}\left(\frac{\partial^2}{\partial x^2}v(x,y)+\frac{\partial^2}{\partial x\,\partial y}u(x,y)\right.\\&\left.+\frac{\partial}{\partial y}w(x,y)\frac{\partial^2}{\partial x^2}w(x,y)+\frac{\partial}{\partial x}w(x,y)\frac{\partial^2}{\partial x\,\partial y}w(x,y)\right)\\&+R_{22}\frac{\partial^2}{\partial y^2}\psi_y(x,y)+R_{12}\frac{\partial^2}{\partial x\,\partial y}\psi_y(x,y)=0,\end{aligned} \tag{53}$$

$$\begin{aligned}\delta w:\;&S_{55}\left(\frac{\partial}{\partial x}\psi_x(x,y)+\frac{\partial^2}{\partial x^2}w(x,y)\right)+S_{44}\left(\frac{\partial}{\partial y}\psi_y(x,y)+\frac{\partial^2}{\partial y^2}w(x,y)\right)\\&+\left(\left(N_{xx}^T+\chi_1N_{xx}^M\right)\frac{\partial^2}{\partial x^2}w(x,y)+\left(N_{yy}^T+\chi_2N_{yy}^M\right)\frac{\partial^2}{\partial y^2}w(x,y)\right)+kw(x,y)\\&-G_\xi\left(\cos^2\theta\frac{\partial^2}{\partial x^2}w(x,y)+2\cos\theta\sin\theta\frac{\partial^2}{\partial x\,\partial y}w(x,y)+\sin^2\theta\frac{\partial^2}{\partial y^2}w(x,y)\right)\\&-G_\eta\left(\sin^2\theta\frac{\partial^2}{\partial x^2}w(x,y)-2\sin\theta\cos\theta\frac{\partial^2}{\partial x\,\partial y}w(x,y)+\cos^2\theta\frac{\partial^2}{\partial y^2}w(x,y)\right)=0,\end{aligned} \tag{54}$$

$$\begin{aligned}\delta\psi_x:\;&H_{11}\frac{\partial^2}{\partial x^2}\psi_x(x,y)+H_{12}\frac{\partial^2}{\partial x\,\partial y}\psi_y(x,y)+H_{66}\left(\frac{\partial^2}{\partial y^2}\psi_x(x,y)+\frac{\partial^2}{\partial x\,\partial y}\psi_y(x,y)\right)\\&-S_{55}\left(\psi_x(x,y)+\frac{\partial}{\partial x}w(x,y)\right)+R_{11}\left(\frac{\partial^2}{\partial x^2}u(x,y)+\frac{\partial}{\partial x}w(x,y).\frac{\partial^2}{\partial x^2}w(x,y)\right)\\&+R_{12}\left(\frac{\partial^2}{\partial x\,\partial y}v(x,y)+\frac{\partial}{\partial y}w(x,y)\frac{\partial^2}{\partial x\,\partial y}w(x,y)\right)\\&+R_{66}\left(\frac{\partial^2}{\partial y^2}u(x,y)+\frac{\partial^2}{\partial x\,\partial y}v(x,y)+\frac{\partial^2}{\partial y^2}w(x,y).\frac{\partial}{\partial x}w(x,y)\right.\\&\left.+\frac{\partial}{\partial y}w(x,y).\frac{\partial^2}{\partial x\,\partial y}w(x,y)\right)=0,\end{aligned} \tag{55}$$

$$\begin{aligned}\delta\psi_y :\ & H_{22}\frac{\partial^2}{\partial y^2}\psi_y(x,y)+H_{12}\frac{\partial^2}{\partial x\,\partial y}\psi_x(x,y)+H_{66}\left(\frac{\partial^2}{\partial x\,\partial y}\psi_x(x,y)+\frac{\partial^2}{\partial x^2}\psi_y(x,y)\right)\\ & -S_{44}\left(\psi_y(x,y)+\frac{\partial}{\partial y}w(x,y)\right)+R_{11}\left(\frac{\partial^2}{\partial x^2}u(x,y)+\frac{\partial}{\partial x}w(x,y).\frac{\partial^2}{\partial x^2}w(x,y)\right)\\ & +R_{22}\left(\frac{\partial^2}{\partial y^2}v(x,y)+\frac{\partial}{\partial y}w(x,y).\frac{\partial^2}{\partial y^2}w(x,y)\right)+R_{12}\left(\frac{\partial^2}{\partial x\,\partial y}u(x,y)\right.\\ & \left.+\frac{\partial}{\partial x}w(x,y)\frac{\partial^2}{\partial x\,\partial y}w(x,y)\right)+R_{66}\left(\frac{\partial^2}{\partial x^2}v(x,y)+\frac{\partial^2}{\partial x\,\partial y}u(x,y)\right.\\ & \left.+\frac{\partial^2}{\partial x\,\partial y}w(x,y).\frac{\partial}{\partial x}w(x,y)+\frac{\partial}{\partial y}w(x,y).\frac{\partial^2}{\partial x\,\partial y}w(x,y)\right)=0,\end{aligned} \tag{56}$$

The CNTRC microplates are considered with three kinds of boundary conditions: all edges simply supported (SSSS) or clamped (CCCC), and two opposite edges simply supported and the other two clamped (SCSC). The boundary conditions are given as follows

SSSS

$$\left.\begin{matrix}x=0\\x=a\end{matrix}\right\}\Rightarrow v=w=\psi_y=0,\ N_x=M_x=0 \tag{57}$$

$$\left.\begin{matrix}y=0\\y=b\end{matrix}\right\}\Rightarrow u=v=w=\psi_x=0,\ N_y=M_y=0 \tag{58}$$

CCCC

$$\left.\begin{matrix}x=0\\x=a\end{matrix}\right\}\Rightarrow u=v=w=\psi_x=\psi_y=0, \tag{59}$$

$$\left.\begin{matrix}y=0\\y=b\end{matrix}\right\}\Rightarrow u=v=w=\psi_x=\psi_y=0. \tag{60}$$

SCSC

$$\left.\begin{matrix}x=0\\x=a\end{matrix}\right\}\Rightarrow v=w=\psi_y=0,\ N_x=M_x=0 \tag{61}$$

$$\left.\begin{matrix}y=0\\y=b\end{matrix}\right\}\Rightarrow u=v=w=\psi_x=\psi_y=0. \tag{62}$$

6. Generalized differential quadrature method

Several numerical methods such as finite element method (FEM), finite difference method (FDM) and GDQM can be employed to solve the boundary value problem. Hence, GDQM is used as a weighted linear sum of the function values at all discrete points chosen in the solution domain of the spatial variable. GDQM is more efficient than the other solution methods. It is more accurate for lower number of grid points (Shu 1999, Ghorbanpour *et al*. 2012b). GDQM is a powerful method, the essence of which is to approximate the partial derivative of a function with respect to a spatial coordinate at a given discrete point, as a weighted linear sum of the function values at all discrete points chosen in the solution domain of the spatial variable. GDQM can easily satisfy a variety of boundary conditions and require much less formulation and programming effort. Recently, GDQM has been extended to handle irregular geometries.

In recent years the GDQM has become increasingly popular in the numerical solution of problems in engineering and physical science. In this method, the differential equations are changed into a first order algebraic equation by employing appropriate weighting coefficients. The weighting coefficients are independent of any special geometry and depend only on the grid spacing. The partial derivatives of a function (say w here) are approximated with respect to specific coordinates (say x and y), at a discrete point in a defined domain ($0<x<a$ and $0<y<b$) as a set of linear weighting coefficients and the amount represented by the function itself at that point and other points throughout the domain. The approximation of the n^{th} and m^{th} derivatives function with respect to x and y, respectively may be expressed in general form (Sepahi *et al*. 2010)

$$\begin{aligned}f_x^{(n)}(x_i,y_i)&=\sum_{k=1}^{N_x}A^{(n)}{}_{ik}\,f(x_k,y_j),\\ f_y^{(m)}(x_i,y_i)&=\sum_{l=1}^{N_y}B^{(m)}{}_{jl}\,f(x_i,y_l),\\ f_{xy}^{(n+m)}(x_i,y_i)&=\sum_{k=1}^{N_x}\sum_{l=1}^{N_y}A^{(n)}{}_{ik}B^{(m)}{}_{jl}\,f(x_k,y_l),\end{aligned} \tag{63}$$

where N_x and N_y, denotes the number of grid points in x and y directions, $f(x,y)$ is the function and $A_{ik}^{(1)}, B_{jl}^{(1)}$ are the weighting coefficients defined as

$$\begin{aligned}A_{ik}^{(1)}&=\frac{M(x_i)}{(x_i-x_j)M(x_j)},\\ B_{jl}^{(1)}&=\frac{P(y_i)}{(y_i-y_j)M(y_j)},\end{aligned} \tag{64}$$

where M and P are Lagrangian operators defined as

$$\begin{aligned}M(x_i)&=\prod_{j=1}^{N_x}(x_i-x_j),\ \ i\neq j\\ P(y_i)&=\prod_{j=1}^{N_y}(y_i-y_j),\ \ i\neq j.\end{aligned} \tag{65}$$

The weighting coefficients for the second, third and fourth derivatives are determined via matrix multiplication,

$$\begin{aligned}&A^{(2)}{}_{ij}=\sum_{k=1}^{N_x}A^{(1)}{}_{ik}A^{(1)}{}_{kj},\ A^{(3)}{}_{ij}=\sum_{k=1}^{N_x}A^{(2)}{}_{ik}A^{(1)}{}_{kj},\ A^{(4)}{}_{ij}=\sum_{k=1}^{N_x}A^{(3)}{}_{ik}A^{(1)}{}_{kj},\quad i,j=1,2,...,N_x,\\ &B^{(2)}{}_{ij}=\sum_{k=1}^{N_y}B^{(1)}{}_{ik}B^{(1)}{}_{kj},\ B^{(3)}{}_{ij}=\sum_{k=1}^{N_y}B^{(2)}{}_{ik}B^{(1)}{}_{kj},\ B^{(4)}{}_{ij}=\sum_{k=1}^{N_y}B^{(3)}{}_{ik}B^{(1)}{}_{kj},\quad i,j=1,2,...,N_y.\end{aligned} \tag{66}$$

Using the following rule, the distribution of grid points in domain is calculated as (Ghorbanpour 2012)

$$\begin{aligned}x_i&=\frac{a}{2}[1-\cos(\frac{\pi i}{N_x})],\\ y_j&=\frac{b}{2}[1-\cos(\frac{\pi j}{N_y})],\end{aligned} \tag{67}$$

Substituting Eq. (63) into the governing Eqs. (52)-(56) yield a set of algebraic equations expressed in matrix form

Table 1 Temperature-dependent material properties of (10, 10) SWCNT (a=b=9.26 nm, R=0.68 nm, h=0.067 nm, Poisson's ratio v_{12}^{CNT}=0.175)

Temperature (K)	$E_{11}^{CNT}=(Tpa)$	$E_{22}^{CNT}=(Tpa)$	$G_{12}^{CNT}=(Tpa)$	$\alpha_{12}^{CNT}=(10^6/K)$	$\alpha_{22}^{CNT}=(10^6/K)$
300	5.6466	7.0800	1.9445	3.4584	5.1682
500	5.5308	6.9348	1.9643	4.5361	5.0189
700	5.4744	6.8641	1.9644	4.6677	4.8943

as follows

$$\left\{\begin{bmatrix} [KL_{1u}] & [KL_{1v}] & [0] & [KL_{1\psi_x}] & [KL_{1\psi_y}] \\ [KL_{2u}] & [KL_{2v}] & [0] & [KL_{2\psi_x}] & [KL_{2\psi_y}] \\ [0] & [0] & [KL_{3w}] & [KL_{3\psi_x}] & [KL_{3\psi_y}] \\ [KL_{4u}] & [KL_{4v}] & [KL_{4w}] & [KL_{4\psi_x}] & [KL_{4\psi_y}] \\ [KL_{5u}] & [KL_{5v}] & [KL_{5w}] & [KL_{5\psi_x}] & [KL_{5\psi_y}] \end{bmatrix} + \begin{bmatrix} [0] & [0] & [KNL_{1w}] & [0] & [0] \\ [0] & [0] & [KNL_{2w}] & [0] & [0] \\ [0] & [0] & [0] & [0] & [0] \\ [0] & [0] & [KNL_{4w}] & [0] & [0] \\ [0] & [0] & [KNL_{5w}] & [0] & [0] \end{bmatrix}\right\} \begin{bmatrix} [u] \\ [v] \\ [w] \\ [\psi_x] \\ [\psi_y] \end{bmatrix} = \begin{bmatrix} [0] \\ [0] \\ [0] \\ [0] \\ [0] \end{bmatrix}, \quad (68)$$

where (KL) and (KNL) are linear and nonlinear coefficients respectively.

The above nonlinear equation can now be solved using GDQM iterative process as follows.

Initially, neglecting nonlinear parameters, which are dependent on displacements, (KNL)=0, Eq. (68) is solved as a linear boundary value problem. This yields the linear buckling load and displacements of CNTRC plate. The displacements are then scaled up. Substituting linear displacements into nonlinear parameters, (KNL) is evaluated. The problem is then solved considering nonlinear terms (KNL) in Eq. (68). This would give the nonlinear displacements and buckling load of the CNTRC plate in the presence of nonlinear parameters. The new nonlinear displacements are scaled up again and the above procedure is repeated iteratively until convergence is achieved.

7. Results and discussion

The numerical solution of nonlinear buckling of CNTRC plates resting on an orthotropic elastomeric temperature-dependent foundation has been carried out using GDQM. The polymer matrix is selected to be Poly methyl methacrylate (PMMA) which has a constant Poisson's ratios of v_m=0.34, temperature-dependent thermal coefficient of $\alpha_m=(1+0.0005\Delta T)\times10^{-6}/K$, temperature-dependent Young moduli of $E_m=(3.52-0.0034T)Gpa$ in which $T=T_0+\Delta T$ and $T_0=300K$ (room temperature). The thickness and width of the CNTRC plate are h=15 μm and b=150 μm respectively. In addition, an arrangement of (10, 10) SWCNTs are used in ten layers as reinforcement, the material properties of which is written in Table 1. The elastomeric medium is made of Poly dimethylsiloxane (PDMS) which is a temperature-dependent material, the properties of which are assumed to be v_s=0.48 and $E_s=(3.22-0.0034T)GPa$ where $T=T_0+\Delta T$ and $T_0=300K$ (room temperature) (Shen 2009).

7.1 Validation

Table 2 Comparisons of dimensionless buckling load parameters obtained in this research with the existing literature presented by Lie *et al*. (2013)

Load Conditions Loading type	Type of CNTRC, Lei *et al*. (2013)			Type of CNTRC, Present work		
	UD	FGO	FGX	UD	FGO	FGX
χ_1=−1, χ_2=0	30.9076	18.7534	40.8005	30.9075	18.7531	40.8003
χ_1=−1, χ_2=−1	9.3805	6.9161	11.4231	9.3804	6.9157	11.4229
χ_1=−1, χ_2=1	89.9909	63.4215	104.9802	89.9906	63.4208	104.9800
χ_1=−1, χ_2=0	46.9779	34.4733	57.3978	46.9768	34.4727	57.3969
χ_1=−1, χ_2=−1	10.3981	8.9197	11.6524	10.3977	8.9189	11.6519
χ_1=−1, χ_2=1	101.0670	81.0655	108.9411	101.0661	81.0644	108.9402
χ_1=−1, χ_2=0	69.3855	48.4971	82.0077	69.3846	48.4961	82.0066
χ_1=−1, χ_2=−1	14.0470	9.3380	15.0540	14.0468	9.3375	15.0534
χ_1=−1, χ_2=1	107.7075	92.2314	113.8593	107.7066	92.2301	113.8581

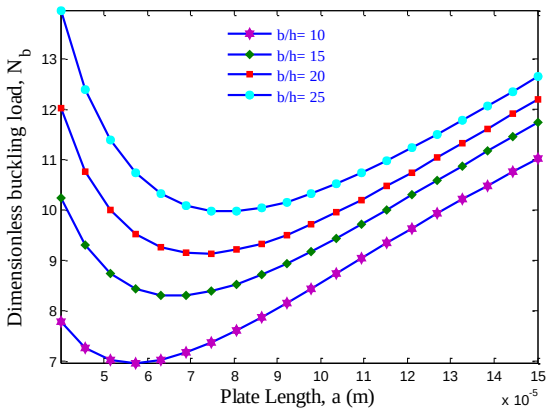

Fig. 2 Effect of aspect ratio on dimensionless buckling load versus length of the CNTRC microplate at uniform distribution of reinforcement (UD)

The validity of the results is demonstrated in comparison with those reported by Lei *et al*. (2013). For this purpose, ignoring the nonlinear terms and elastomeric medium, the non-dimensional buckling load parameter (i.e., $\bar{N}_{cr}=N_{cr}L_y^2/E_mh^3$) of the CNTRC plate with simply supported boundary condition are written in Table 2 considering material properties the same as Lei *et al*. (2013).

Three loading conditions are considered namely as uniaxial compression (i.e., χ_1=−1, χ_2=0), biaxial compression (i.e., χ_1=−1, χ_2=−1) and biaxial compression and tension (i.e., χ_1=−1, χ_2=1)). As can be seen, our results obtained by GDQM are in good agreement with those reported by Lei *et al*. (2013) based on the element-free kp-Ritz method.

7.2 Nonlinear buckling of CNTRC microplate

Dimensionless buckling load of CNTRC microplate (i.e., $N_b=N_{ii}^M/C_{11m}h\ \ (i=x,y)$) for the case of biaxial compression (i.e., χ_1=−1, χ_2=−1)) is plotted versus the plate length for different aspect ratios (width to thickness, b/h), boundary conditions, foundation type, temperature,

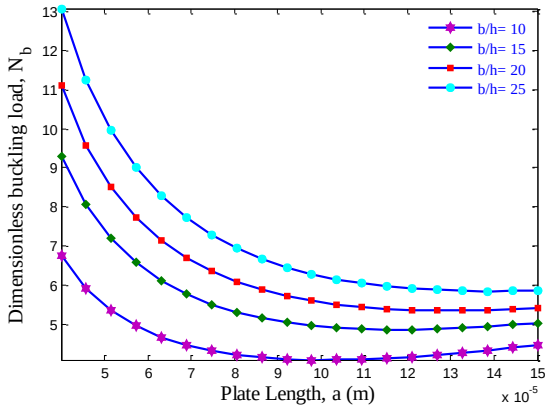

Fig. 3 Effect of aspect ratio on dimensionless buckling load versus length of the CNTRC microplate at non-axisymmetric distribution of reinforcement (NAFG)

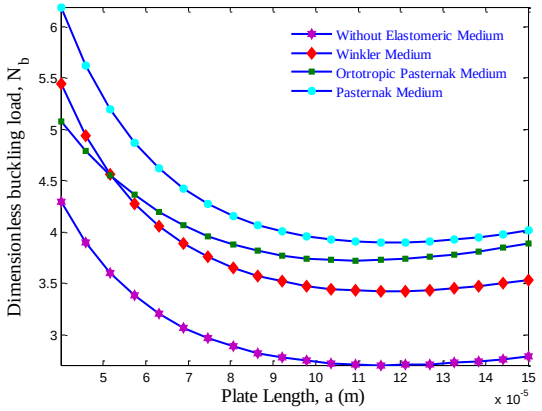

Fig. 6 The effect of elastomeric temperature-dependent foundations of CNTRC microplate on nonlinear buckling load versus length of the microplate

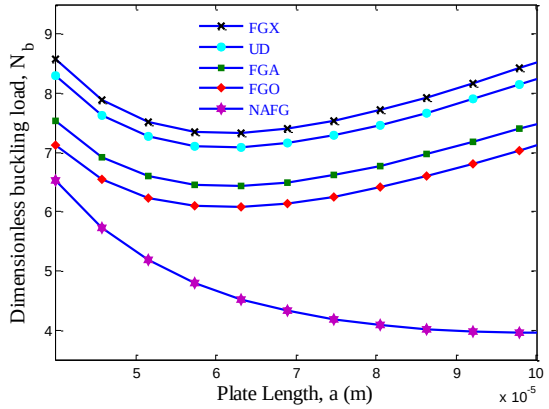

Fig. 4 Dimensionless buckling load versus length of CNTRC microplate for different functionally graded distributions of reinforcement (FG)

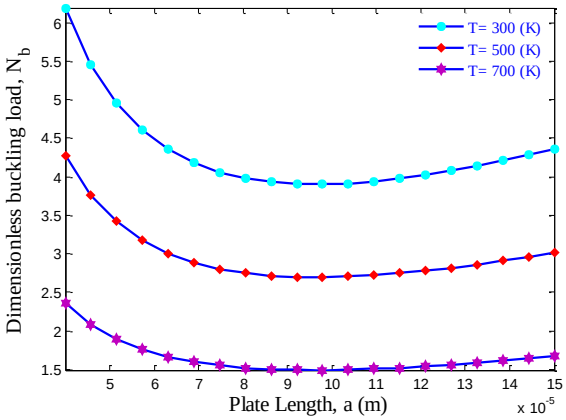

Fig. 7 The effect of temperature of CNTRC microplate on dimensionless buckling load versus length of the microplate

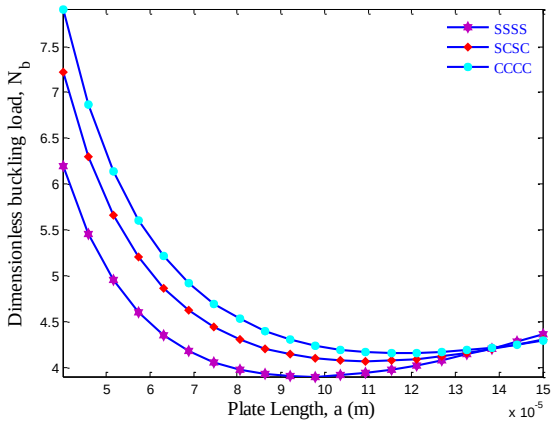

Fig. 5 The effect of boundary condition of CNTRC microplate on dimensionless buckling load versus length of the microplate

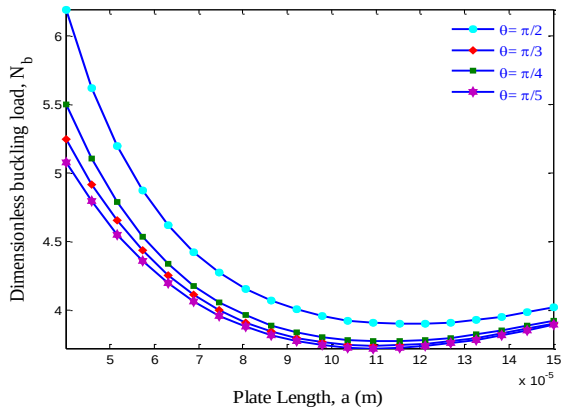

Fig. 8 Dimensionless buckling load versus length of CNTRC microplate for different orientation angle of orthotropic elastomeric foundation

reinforcement fibers distribution arrangements and orthotropic shear orientation angle.

Fig. 2, for the case of simply supported boundary condition (SSSS), illustrates the nonlinear buckling load versus length of CNTRC microplate for four different aspect ratios (width to thickness, *b*/*h*). In this plot the uniform distribution (UD) arrangement of SWCNTs is considered. It is clear from this figure that, for the same microplate length, the minimum dimensionless buckling load in biaxial compression belongs to the lowest aspect ratio of 10 (*b*/*h*=10). This is due to the slenderness and lower stiffness of microplate in this case. As expected, for the same microplate length, increasing aspect ratio will increase critical buckling load.

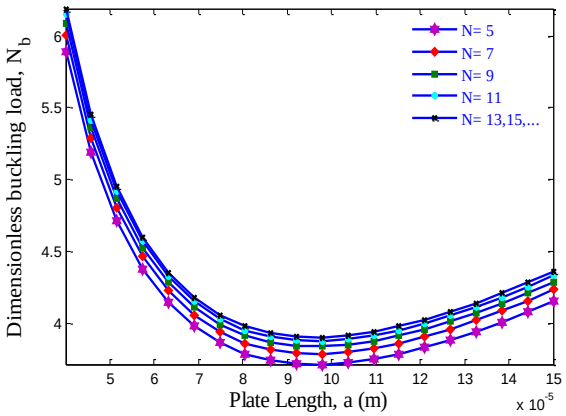

Fig. 9 Number of grid points effect on the convergence and accuracy of the results obtained by GDQM

Fig. 3 demonstrates the dimensionless nonlinear buckling load versus length of CNTRC microplate with SSSS boundary condition for four different aspect ratios and non-axisymmetric functionally graded (NAFG) distribution of SWCNTs. It is obvious from the plot that the buckling load is decreasing by increasing the microplate length. Again, for the same microplate length, the lowest dimensionless buckling load belongs to the lowest aspect ratio. Although the effect of aspect ratio on dimensionless buckling load for both NAFG and UD distributions of SWCNTs is almost similar at the same microplate length, but It can be found that the distribution arrangements of SWCNTs have significant influence on the magnitude of buckling load. In general, for the case of NAFG, the buckling load is lower than uniform distribution (UD) particularly for higher plate lengths.

Fig. 4 illustrates the effect of SWCNT distribution in microplate, for the SSSS boundary condition, on the dimensionless buckling load versus length of the CNTRC microplate. This figure is plotted for the aspect ratio of 10 (b/h=10). For the CNTRC microplate, UD and four types of FG distribution patterns of SWCNT reinforcements are assumed. It should be noted that the mass fraction (w_{CNT}) of the UD and FG distribution of CNTs in polymer are considered to be equal for the purpose of comparisons. As can be seen, the buckling load for the FGA, FGO and NAFG cases are lower than the buckling load of UD microplates. While the FGX microplate has higher buckling load than four other cases. It is due to the fact that the stiffness of CNTRC microplates changes with the arrangement of CNTs distribution in polymer matrix. However, it can be concluded that SWCNT distribution close to the top and bottom of the microplate are more efficient than those distributed near the mid-plane because of increasing stiffness of the microplate.

It also resulted that the NAFG distribution of SWCNs leads to a significant effect on dimensionless buckling load of the microplate and is less than other distribution cases. Generally, for the case of NAFG, the dimensionless buckling load is lower than other distribution cases particularly for higher microplate lengths.

Fig. 5 shows the dimensionless buckling load versus length of the CNTRC microplate for different boundary conditions. It can be found that the dimensionless buckling load of microplate with clamped boundary condition at four edges (CCCC), defined by Eqs. (59)-(60), is greater than other boundary condition. Moreover, the dimensionless buckling load of SCSC boundary condition of the microplate is located between the buckling load of CCCC and SSSS cases for the same aspect ratio of 10 (b/h=10). This is due to the fact that the CNTRC microplate with CCCC boundary condition has higher stiffness with respect to other boundary conditions.It may be mentioned that the effect of boundary condition for lower length of the microplate is more significant than higher microplate length. On the other hand the dimensionless buckling loads in longer microplate length are almost identical for all boundary conditions.

The dimensionless buckling load of the CNTRC microplate versus length is demonstrated in Fig. 6 for different elastomeric foundation mediums. In this figure, four cases are considered as follows:

Case 1: Considering dimensionless buckling load in the absence of elastomeric medium.

In this case, the dimensionless buckling load is significantly lower than other cases in which elastomeric temperature-dependent mediums are considered.

Case 2: Considering elastomeric Winkler medium.

The normal foundation effect of elastomeric medium on the bottom surface of the microplate is simulated as Winkler type defined by Eq. (28).

Case 3: Considering elastomeric orthotropic medium.

In this case both Winkler and Pasternak constants are considered. Also θ=45° is considered for Pasternak shear model orientation of orthotropic medium.

Case 4: Considering elastomeric Pasternak medium.

In this case, only Pasternak constant is considered. It is obvious from Fig. 6 that the dimensionless buckling load of the microplate is increased due to stiffer structure of the plate rested on the elastomeric foundation.

Moreover, The Pasternak elastomeric foundation model is more efficient than other foundation types. This is because both normal and shear effects are taken into account in this case.

Fig. 6 also shows that the minimum dimensionless buckling load belongs to case 1 which is expected. The dimensionless buckling load of the microplate in the other two cases, Winkler and orthotropic Pasternak, are located between these two extremes. For lower length of the microplate, the effect of Winkler and orthotropic Pasternak foundations is not significant.

Dimensionless buckling load versus length of CNTRC microplate for different orientation angle of foundation orthotropy, for NAFG-type, is shown in Fig. 8. Note that, the foundation parameters are selected to be K_W=41.4 N/m^3, G_ξ=41.4 N/m and G_η=4.14 N/m. As can be seen, orientation angle of foundation orthotropy do not have direct effect on the nonlinear buckling load of the CNTRC microplate.

Generally, decreasing the orientation angle of the foundation orthotropy, decreases the dimensionless buckling load. The convergence and accuracy of the numerical procedure (GDQM) in evaluating the dimensionless buckling load of the CNTRC microplate for

different number of grid points is shown in Fig. 9. Indeed, increasing the number of grid points will yield more accuracy. However, efficiency and accuracy of the procedure will not be changed considerably for more than 11×11 grid points. For this reason a number of 11×11 grid points is chosen in our solution.

8. Conclusions

Nonlinear buckling behavior of a nano-composite microplate made of polymer based matrix reinforced by several arrangements of carbon nanotubes including non-axisymmetric distribution is investigated. The microplate is rested on an elastomeric temperature dependent foundation considering Winkler and orthotropic Pasternak effects. Three different combinations of simply supported and clamped edge boundary conditions are considered. Heat conduction equation is solved to obtain temperature distribution along thickness of the plate. The set of governing differential equations of the microplate is derived using nonlinear Mindlin displacement theory, energy method and Hamilton principle. It has been found that the orthotropic elastomeric foundation has a significant effect on buckling load of the microplate. Moreover, for non-axisymmetric distribution of reinforcement, the buckling load is lower than all other arrangements. It has also been concluded that the buckling load in longer microplate length is almost identical for all edge boundary conditions.

References

Akhavan, H., Hosseini Hashemi, S., Rokni Damavandi Taher, H., Alibeigloo, A. and Vahabi, S. (2009), "Exact solutions for rectangular mindlin plates under in-plane loads resting on Pasternak elastic foundation, part II: Frequency analysis", *Comput. Mater. Sci.*, **44**(3), 951-961.

Baltacıoğlu, A.K., Civalek, Ö., Akgöz, B. and Demir, F. (2011), "Large deflection analysis of laminated composite plates resting on nonlinear elastic foundations by the method of discrete singular convolution", *J. Press. Vessel. Pip.*, **88**(8), 290-300.

Esawi, A.M.K. and Farag, M.M. (2007), "Carbon nanotube reinforced composites: Potential and current challenges", *Mater. Des.*, **28**(9), 2394-2401.

Ferreira, A.J.M., Roque, C.M.C. and Martins, P.A.L.S. (2003), "Analysis of composite plates using higher-order shear deformation theory and a finite point formulation based on the multiquadric radial basis function method", *Compos. Part B*, **34**(7), 627-636.

Fiedler, B., Gojny, F.H., Wichmann, M.H.G., Nolte, M.C.M. and Schulte, K. (2006), "Fundamental aspects of nano-reinforced composites", *Compos. Sci. Technol.*, **66**(16), 3115-3125.

Fiorenzo, A.F. (2015), "Natural frequencies and critical temperatures of functionally graded sandwich plates subjected to uniform and non-uniform temperature distributions", *Compos. Struct.*, **121**, 197-210.

Ghorbanpour Arani, A., Kolahchi, R. and Mosallaie Barzoki, A.A. (2011), "Effect of material in-homogeneity on electro-thermo-mechanical behaviors of functionally graded piezoelectric rotating shaft", *Appl. Math. Model.*, **35**(6), 2771-2789.

Ghorbanpour Arani, A., Kolahchi, R., Mosallaie Barzoki, A.A. and Loghman, A. (2012a), "Electro-thermo-mechanical behaviors of FGPM spheres using analytical method and ANSYS software", *Appl. Math. Model.*, **36**(1), 139-157.

Ghorbanpour Arani, A., Kolahchi, R., Mosallaie Barzoki, A.A., Mozdianfard, M.R. and Noudeh Farahani, M. (2012b), "Elastic foundation effect on nonlinear thermo-vibration of embedded double-layered orthotropic grapheme sheets using differential quadrature method", *J. Mech. Eng. Sci.*, **227**(4), 862-879.

Ghorbanpour Arani, A., Mosallaie Barzoki, A.A. and Kolahchi, R. (2014), "Nonlinear dynamic buckling of viscous-fluid-conveying PNC cylindrical shells with core resting on visco-Pasternak medium", *J. Sol. Mech.*, **6**(3), 265-277.

Groh, R.M.J. and Weaver, P.M. (2014), "Buckling analysis of variable angle tow variable thickness panels with transverse shear effects", *Compos. Struct.*, **107**, 482-493.

Huu-Tai, T. and Thuc, P.V. (2013), "A new sinusoidal shear deformation theory for bending, buckling and vibration of functionally graded plates", *Appl. Math. Model.*, **37**(5), 3269-3281.

Jafari Mehrabadi, S., Sobhani Aragh, B., Khoshkhahesh, V. and Taherpour, A. (2012), "Mechanical buckling of nanocomposite rectangular plate reinforced by aligned and straight single-walled carbon nanotubes", *Compos. Part B: Eng.*, **43**(4), 2031-2040.

Kiani, Y. and Eslami, M.R. (2013), "An exact solution for thermal buckling of annular FGM plates on an elastic medium", *Compos. Part B*, **45**(1), 101-110.

Kutlu, A. and Omurtag, M.H. (2012), "Large deflection bending analysis of elliptic plates on orthotropic elastic foundation with mixed finite element method", *J. Mech. Sci.*, **65**(1), 64-74.

Lee, Y.Y., Zhao, X. and Reddy, J.N. (2010), "Postbuckling analysis of functionally graded plates subject to compressive and thermal loads", *Comput. Meth. Appl. Mech. Eng.*, **199**(25), 1645-1653.

Lei, Z.X., Liew, K.M. and Yu, J.L. (2013), "Buckling analysis of functionally graded carbon nanotube-reinforced composite plates using the element-free kp-ritz method", *Compos. Struct.*, **98**, 160-168.

Morozov, N.F. and Tovstik, P.E. (2010), "On modes of buckling for a plate on an elastic foundation", *Mech. Sol.*, **45**(4), 519-528.

Mosallaie Barzoki, A.A., Ghorbanpour Arani, A., Kolahchi, R. and Mozdianfard, M.R. (2012), "Electro-thermo-mechanical torsional buckling of a piezoelectric polymeric cylindrical shell reinforced by DWBNNTs with an elastic core", *Appl. Math. Model.*, **36**(7), 2983-2995.

Mosallaie Barzoki, A.A., Ghorbanpour Arani, A., Kolahchi, R., Mozdianfard, M.R. and Loghman, A. (2013), "Nonlinear buckling response of embedded piezoelectric cylindrical shell reinforced with BNNT under electro-thermo-mechanical loadings using HDQM", *Compos. Part B*, **44**(1), 722-727.

Mosallaie Barzoki, A.A., Loghman, A. and Ghorbanpour Arani, A. (2015), "Temperature-dependent nonlocal nonlinear buckling analysis of functionally graded SWCNT-reinforced microplates embedded in an orthotropic elastomeric medium", *Struct. Eng. Mech.*, **53**(3), 497-517.

Ovesy, H.R., Totounferoush, A. and Ghannadpour, S.A.M. (2015), "Dynamic buckling analysis of delaminated composite plates using semi-analytical finite strip method", *J. Sound Vibr.*, **343**(12), 131-143.

Piovan, M.T., Domini, S. and Ramirez, J.M. (2012), "In-plane and out-of-plane dynamics and buckling of functionally graded circular curved beams", *Compos. Struct.*, **94**(11), 3194-3206.

Reddy, J.N. (1984), "A simple higher order theory for laminated composite plates", *J. Appl. Mech.*, **51**(4), 745-752.

Salvetat-Delmotte, J.P. and Rubio, A. (2002), "Mechanical properties of carbon nanotubes: A fiber digest for beginners", *Carbon*, **40**(10), 1729-1734.

Sepahi, O., Forouzan, M.R. and Malekzadeh, P. (2010), "Large

deflection analysis of thermo-mechanical loaded annular FGM plates on nonlinear elastic foundation via DQM", *Compos. Struct*., **92**(10), 2369-2378.

Shen, H.S. (2009), "Nonlinear bending of functionally graded carbon nanotube-reinforced composite plates in thermal environments", *Compos. Struct.*, **91**(1), 9-19.

Shen, H.S. and Zhang, C.L. (2011), "Nonlocal beam model for nonlinear analysis of carbon nanotubes on elastomeric substrates", *Comput. Mater. Sci*., **50**(3), 1022-1029.

Shu, C. (1999), *Differential Quadrature and Its Application in Engineering*, Springer.

Swaminathan, K. and Ragounadin, D. (2004), "Analytical solutions using a higher-order refined theory for the static analysis of antisymmetric angle-ply composite and sandwich plates", *Compos. Struct*., **64**(3), 405-417.

SF